ÄSPÖLABORATORIET

INTERNATIONAL COOPERATION REPORT 94-08

Application of three-dimensional smeared fracture model to the groundwater flow and the solute migration of LPT-2 experiment

T Igarashi, Y Tanaka, M Kawanishi

Abiko Research Laboratory, Central Research Institute of Electric Power Industry, Abiko, Japan

October 1994

Supported by CRIEPI, Japan

SVENSK KÄRNBRÄNSLEHANTERING AB
SWEDISH NUCLEAR FUEL AND WASTE MANAGEMENT CO

BOX 5864 S-102 40 STOCKHOLM

TEL. +46-8-665 28 00 TELEX 13108 SKB TELEFAX +46-8-661 57 19

9505310298 950424
PDR WASTE
WM-11 PDR

Recd and letter etc
4/24/95

ISSN 1104-3210
ISRN SKB-ICR--94/8--SE

APPLICATION OF THREE-DIMENSIONAL SMEARED FRACTURE MODEL TO THE GROUNDWATER FLOW AND THE SOLUTE MIGRATION OF LPT-2 EXPERIMENT

T Igarashi, Y Tanaka, M Kawanishi

Abiko Research Laboratory, Central Research Institute of Electric Power Industry, Abiko, Japan

October 1994

Supported by CRIEPI, Japan

This document concerns a study which was conducted within an Äspö HRL joint project. The conclusions and viewpoints expressed are those of the author(s) and do not necessarily coincide with those of the client(s). The supporting organization has reviewed the document according to their documentation procedure.

102-8

APPLICATION OF THREE-DIMENSIONAL SMEARED FRACTURE MODEL TO THE GROUNDWATER FLOW AND THE SOLUTE MIGRATION OF LPT-2 EXPERIMENT

T Igarashi, Y Tanaka, M Kawanishi

Abiko Research Laboratory
Central Research Institute of Electric Power Industry, Abiko, Japan

October 1994

Keywords : SMEARED FRACTURE MODEL, THREE-DIMENSIONAL ANALYSIS, LONG-TERM PUMPING TEST, GROUNDWATER FLOW, SOLUTE MIGRATION, FRACTURE, ROCK MATRIX, FINITE-ELEMENT METHOD

EXECUTIVE SUMMARY

A three-dimensional smeared fracture model was applied to groundwater flow and tracer migration during the LPT-2 experiment. The smeared fracture model, which offered several of the advantages of a discrete fracture model and a porous media model, was combined with a three-dimensional groundwater flow simulation code called FEGM and a three-dimensional solute migration simulation code called FERM. These codes calculate both steady-state and unsteady-state conditions based on the finite-element method. Hydraulic parameters such as permeability coefficients and specific storage coefficients of finite-element meshes intersecting fractures are calculated with volume-weighted values of the fractures and the matrix by using this model so that complex fractured configurations could easily be treated.

The entire island of Aspo was included in the region for groundwater flow analysis, while the area in the vicinity of the pumping borehole KAS06 was taken out for tracer migration analysis. The input parameters were determined according to the conceptual model constructed by SKB.

The simulated results of the steady-state groundwater flow agreed fairly well with the final measured drawdowns during pumping at KAS06, although considerable discrepancies in drawdown were found in several sections, as shown in Fig.1. Furthermore, the simulated results were not greatly dependent upon the total number of finite elements. This indicates that the smeared fracture model is effective, since the use of an enormous number of finite-element meshes is not needed when simulating an approximate groundwater flow through fractured media. The considerable disagreement found in several sections may be due to differences in connectivity between the smeared fracture network used here and the real fracture network. The simulated results of the unsteady-state groundwater flow were largely dependent on the mesh diagram used as well as the specific storage coefficients of the fractures. It is possible to evaluate the specific storage coefficient of each fracture by fitting the simulated drawdown curves to the observed ones more closely, although a rough estimate of the coefficient was obtained by assuming the same coefficient for all the fractures.

A particle pathway from KAS08, M1 to KAS06 was selected for tracer migration analysis because of a relatively short Darcian time. The trajectories are illustrated in Fig.2. This indicates that several fractures may be involved in the tracer migration from KAS08, M1 to KAS06. The simulated breakthrough curve of the tracer, Rhenium-186, in the groundwater of KAS06 was in good agreement with the observed one, assuming that the tracer recovery ratio

was 10%, as shown in Fig.3. This suggests that more water-conductive zones intersect the tracer injection borehole, the pumping borehole and/or the related fracture zones than first considered, reducing the recovery of the injected tracer.

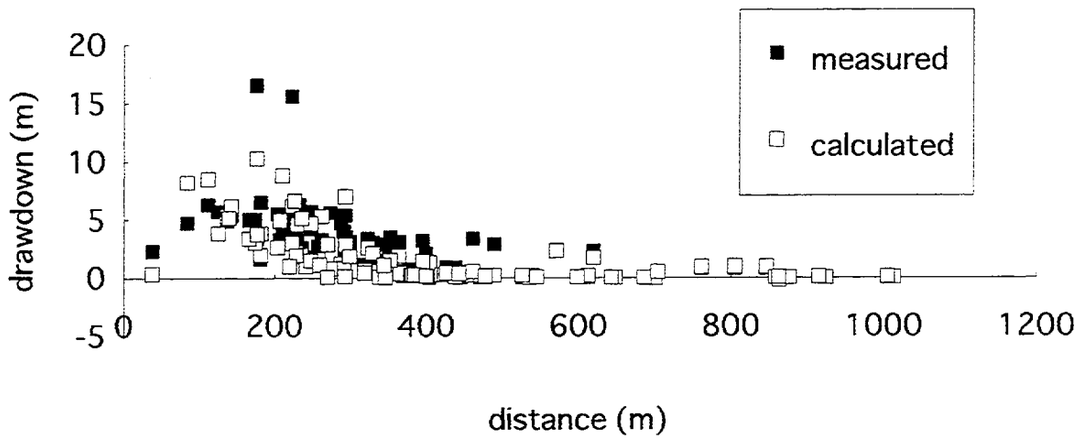

Fig. 1(a) Calculated drawdowns from steady-state analysis using coarse mesh diagram compared with measured drawdowns

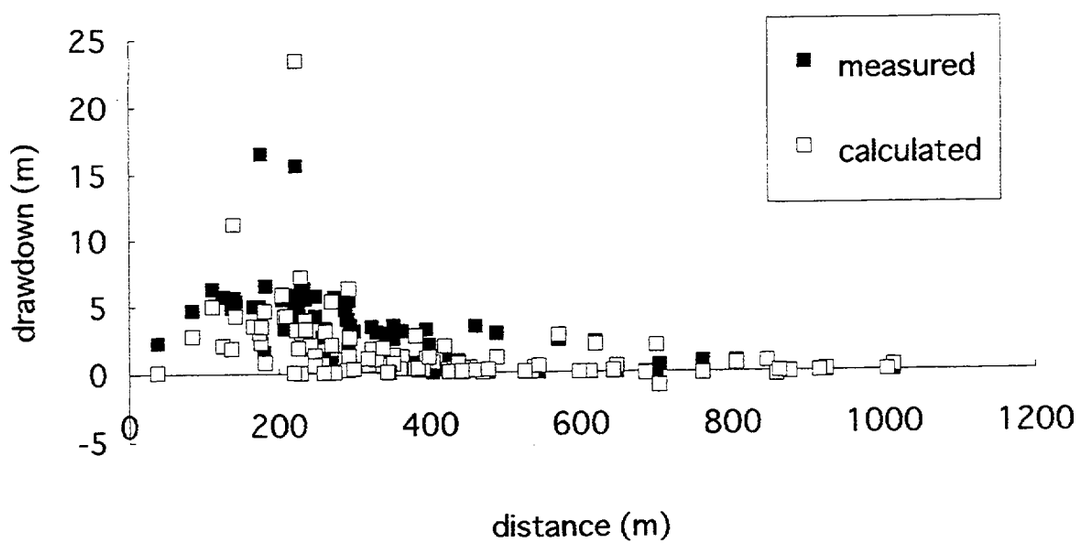

Fig. 1(b) Calculated drawdowns from steady-state analysis using fine mesh diagram compared with measured drawdowns

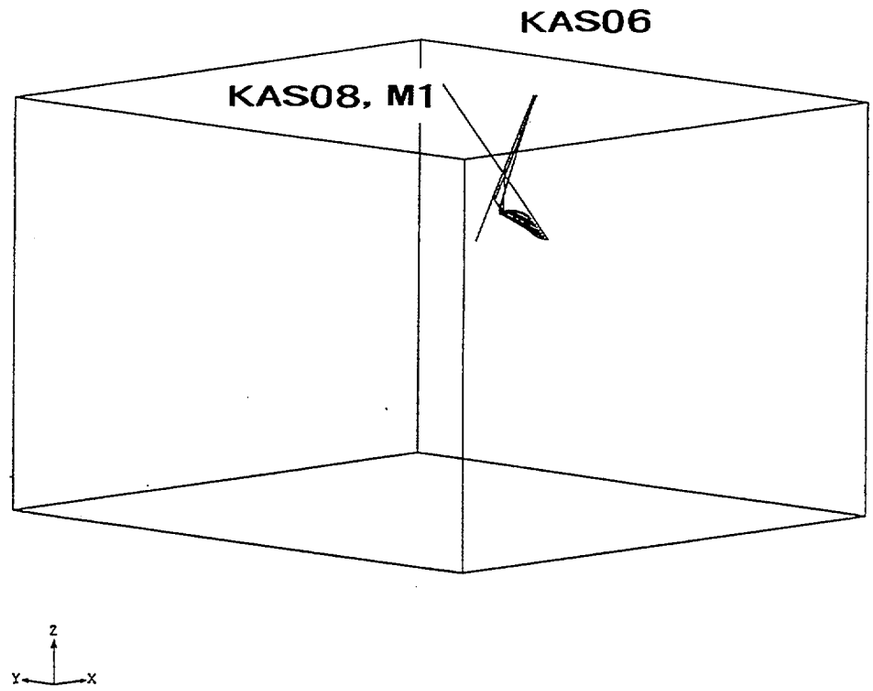

Fig. 2 Trajectories from KAS08, M1 to KAS06 from steady-state analysis using fine mesh diagram

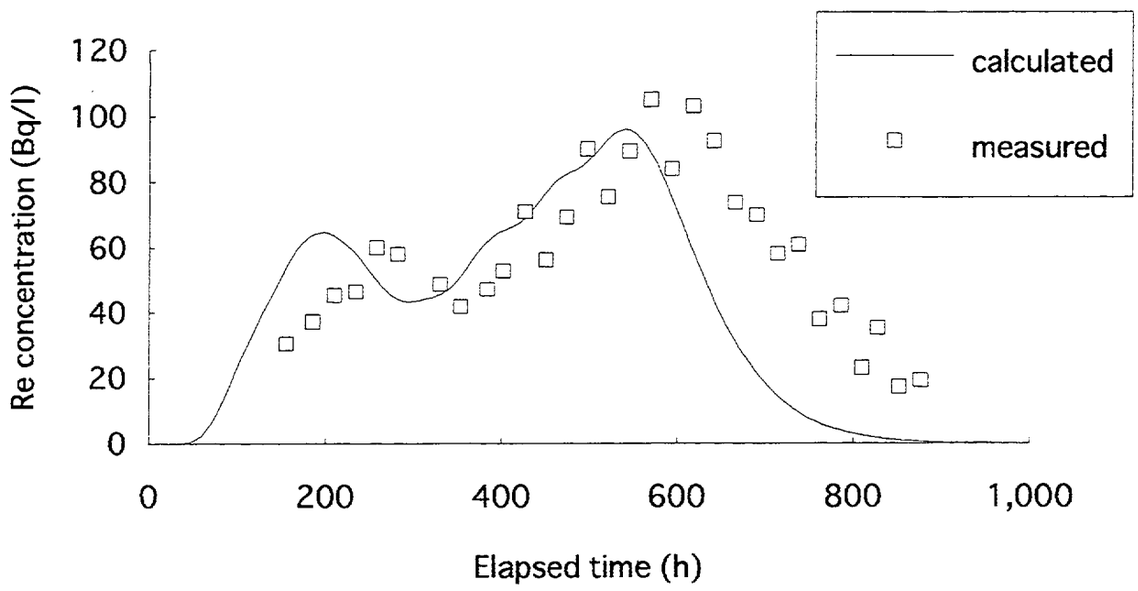

Fig. 3 Calculated breakthrough curve corrected for recovery of Rhenium-186 and measured breakthrough curve at sampling level 190m in KAS06

ABSTRACT

A three-dimensional smeared fracture model was applied to groundwater flow and tracer migration during the LPT-2 experiment. The smeared fracture model, which offered several of the advantages of a discrete fracture model and a porous media model, was combined with a groundwater flow simulation code called FEGM and a solute migration simulation code called FERM. These codes calculate both steady-state and unsteady-state conditions based on the finite-element method. Hydraulic parameters such as permeability coefficients and specific storage coefficients of finite-element meshes intersecting fractures are calculated with volume-weighted values of the fractures and the matrix by using this model so that complex fractured configurations could easily be treated.

The entire island of Aspo was included in the region for groundwater flow analysis, while the area in the vicinity of the pumping borehole KAS06 was taken out for tracer migration analysis.

The simulated results of the steady-state groundwater flow agreed fairly well with the measured drawdowns, although considerable discrepancies in drawdown were found in several sections. Furthermore, the simulated results were not greatly dependent upon the total number of finite elements. This indicates that the smeared fracture model is effective, since the use of an enormous number of finite-element meshes is not needed when simulating an approximate groundwater flow through fractured media. The considerable disagreement found in several sections may be due to differences in connectivity between the smeared fracture network used here and the real fracture network. The simulated results of the unsteady-state groundwater flow were largely dependent on the mesh diagram used as well as the specific storage coefficients of the fractures. It is possible to evaluate the specific storage coefficient of each fracture by fitting the simulated drawdown curves to the observed ones more closely .

A particle pathway from KAS08, M1 to KAS06 was selected for tracer migration analysis because of a relatively short Darcian time. The calculated trajectories indicate that several fractures may be involved in the pathway. The simulated breakthrough curve of the tracer, Rhenium-186, in the groundwater of KAS06 was in good agreement with the observed one, assuming that the tracer recovery ratio was 10%. This suggests that more water-conductive zones than first considered reduce the recovery of the injected tracer.

CONTENTS

		Page
1	INTRODUCTION	1
2	DESCRIPTION OF MODEL APPLIED	2
2.1	Groundwater flow model	2
2.2	Solute migration model	2
2.3	Smeared fracture model	3
3	INPUT PARAMETERS AND CONDITIONS	8
3.1	Groundwater flow conditions	8
3.2	Tracer migration conditions	8
4	RESULTS OF SIMULATION	14
4.1	Groundwater flow simulation	14
4.2	Tracer migration simulation	15
5	SUMMARIES	32
	REFERENCES	33
	APPENDIX	34

1 INTRODUCTION

In 1990, SKB conducted a long-term pumping test and a subsequent tracer test called LPT-2 to identify major water-conductive structures on Aspo /Rhen *et al.*, 1992/. KAS06, which is located on the southern part of Aspo island and is 602 m long, was used as a pumping borehole. Five boreholes - KAS02, KAS05, KAS07, KAS08 and KAS12 - were selected as tracer injection boreholes. The groundwater pressure change due to pumping was measured in the surrounding boreholes in Aspo, and the tracer concentration change in the groundwater sampled from KAS06 was also measured.

There are several major water-conductive zones in Aspo /Wikberg *et al.*, 1991/. It is difficult to model all conductive zones with definitely determined coordinates in three dimensions. We applied a smeared fracture model to groundwater flow and tracer migration analysis in fractured media such as Aspo to simplify the input data and to obtain an approximate solution efficiently, and the appropriateness of the model was examined.

2 DESCRIPTION OF MODEL APPLIED

2.1 Groundwater flow model

The groundwater flow simulation code called FEGM (Finite-Element model of Groundwater Movement) was applied to the LPT-2 experiment. Its original form is an unsaturated/ saturated vertical two-dimensional flow model developed by Yeh *et al.* /1979/. The spatial dimensions of the model and the solvers of algebraic equations transformed by a finite-element numerical approximation of the model were modified by Kawanishi *et al.* /1987/, Kawanishi *et al.* /1994/ and Shimogaki *et al.* /1993/. The modification of the model is summarized in Table 2.1. The heterogeneity of the groundwater flow can only be expressed by using different values of parameters such as the permeability coefficient and the specific storage coefficient for specific elements compared with those for the surrounding elements. The governing equation of the model is expressed as follows;

$$F \frac{\partial h}{\partial t} = \nabla \cdot [\, K \nabla H \,] + Q$$

$$F = \theta \beta' + d\theta / dh + \theta / n \cdot \alpha'$$

where F denotes a generalized specific storage coefficient, h pressure head, t time, K hydraulic conductivity tensor, H total head, Q sink/source term, θ volumetric water content, β' compressibility of water, n porosity, and α' compressibility of media.

The characteristics of the groundwater flow model are briefly described in Table 2.2. Further details of the model are also described in an appendix.

2.2 Solute migration model

The solute migration simulation code called FERM (Finite-Element model of Radionuclide Migration) was applied to tracer migration during the LPT-2 experiment. Its original form is a vertical two-dimensional solute transfer model developed by Yeh *et al.* /1981/. The spatial dimensions, the adsorption models of solutes, and the solvers of algebraic equations transformed by a finite-element numerical approximation were also modified by Kawanishi *et al.* /1987/, Kawanishi *et al.* /1994/, and Shimogaki *et al.* /1993/. The modification of the model is also summarized in Table 2.1. The heterogeneity of the solute migration can only be expressed by using different values of parameters such as the distribution coefficient and the dispersion coefficient for specific elements compared with those for the surrounding elements. The governing equation of the model is expressed as follows;

$$(\theta+\rho_b K_d)\frac{\partial C}{\partial t}+\nabla(VC)-\nabla\cdot[\theta D\nabla C]$$
$$+\lambda(\theta+\rho_b K_d)C+(K_w\theta+K_s\rho_b K_d)C-M=0$$
$$\theta D=a_L|V|\delta ij+(a_L-a_T)Vi\,Vj/|V|+a_m\tau\delta ij\theta$$

where C denotes solute concentration, ρ_b bulk density, K_d distribution coefficient, V Darcy velocity calculated by FEGM, D dispersion coefficient, λ decay constant, Kw rate coefficient with respect to liquid phase, Ks rate coefficient with respect to solid phase, M sink/source term, a_L longitudinal dispersivity, a_T lateral dispersivity, δ_{ij} Kronecker delta, a_m diffusion coefficient, and τ tortuosity.

The characteristics of the solute migration model are briefly described in Table 2.3. Further details of the model are also described in an appendix. Adsorption of the tracer used and rate coefficients for physical, chemical or biological reactions were ignored in the calculation.

2.3 Smeared fracture model

A smeared fracture model was coupled with FEGM and FERM and was applied to fractured media such as are found in Aspo island in order to model a heterogeneous field for analysis of groundwater flow and solute migration. According to the smeared fracture model, when a fracture intersects several finite elements as shown in Fig.2.1, the parameters within the elements are approximated to area-weighted values of the fracture and the matrix for two-dimensional analysis, and to volume-weighted values for three-dimensional analysis. The model also deals with anisotropy of permeability and dispersivity depending on the direction of the fracture. Therefore, the smeared fracture model, which offers several of the advantages of a discrete fracture model and a porous media model, improves the modelling of heterogeneous fracture networks, although the fractures expressed by this model have a jagged shape. On the other hand, the smeared fracture model approaches the discrete fracture model as the mesh size of the elements decreases.

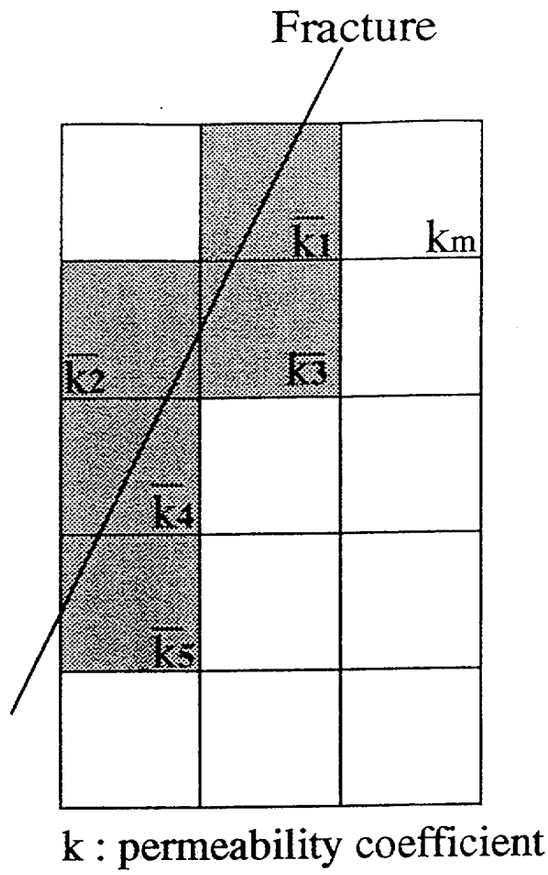

Fig. 2.1 Concept of smeared fracture model

Table 2.1 The differences between FEMWATER/FEMWASTE and FEGM/FERM

	FEMWATER / FEMWASTE	FEGM / FERM
Dimension	Vertical two dimension	Vertical two dimension
		Horizontal two dimension
		Quasi-three dimension
		Three dimension
Adsorption model	Equilibrium Henry model	Equilibrium Henry model
		Equilibrium Langmuir model
		Equilibrium Freundlich model
		Kinetic Henry model
		Kinetic Langmuir model
		Kinetic Freundlich model
Matrix solver	Banded matrix method	Banded matrix method
		Skyline matrix method
		Conjugate gradient method

Table 2.2 Condensed description of the groundwater flow model of the Aspo site used by CRIEPI

CRIEPI'S GROUNDWATER FLOW MODEL OF THE ASPO SITE Porous media model with smeared fractures	
Process description Continuity description (mass rate) Equation of motion (Darcy's law including unsaturated infiltration)	
CONCEPT	DATA
Geometric framework and parameters	
3D box divided into 14020 and 104040 Sixteen 2D fracture zones, planar with limited extent (location, orientation, size)	Size : 1.8*2.0*1.3 km Fracture network based on the conceptual model constructed by SKB
Material properties	
Transmissivity or hydraulic conductivity Specific storage coefficient	Transmissivity based on the values estimated by SKB
Spatial assignment model	
Transmissivity : Deterministic assignment Elements crossing fractures calculated as volume-weighted in properties	Transmissivity based on the values estimated by SKB
Boundary conditions	
Upper : Fixed pressure head on Aspo constant head at sea Lower : No flow Side : Prescribed pressure (hydrostatic) Salinity : Constant	Contour map data
Numerical tool FEGM	
Output parameters Pressure head, total head, Darcy velocity, trajectories, flux	

Table 2.3 Condensed description of the tracer migration model of the Aspo site used by CRIEPI

CRIEPI'S TRACER MIGRATION MODEL OF THE ASPO SITE Porous media model with smeared fractures	
Process description Mass balance description (convection, dispersion, diffusion, adsorption, decay, and decomposition)	
CONCEPT	DATA
Geometric framework and parameters	
3D box divided into 88000 2D fracture zones, planar with limited extent (location, orientation, size)	Size : 0.4*(0.3-0.45)*0.5 km Fracture network based on the conceptual model constructed by SKB
Material properties	
Darcy velocities Dispersivity Diffusion coefficient, distribution coefficient, decay constant, reaction rate constant	Darcy velocities calculated by FEGM Dispersivity estimated by SKB not used
Spatial assignment model	
Dispersivity : Deterministic assignment Elements crossing fractures calculated as volume-weighted in properties	Dispersivity based on the value estimated by SKB
Boundary conditions	
Upper, side : Concentration gradient equal to zero	
Numerical tool FERM	
Output parameters Concentration distribution at a specific time, concentration change at a specific point	

3 INPUT PARAMETERS AND CONDITIONS

3.1 Groundwater flow conditions

The region of the groundwater flow simulation during the LPT-2 experiment adopted here conformed to the model by Svensson /1991a/. The mesh diagram is shown in Fig.3.1. Two different kinds of diagram were constructed: one is a coarse mesh diagram (14,020 elements) and the other a fine mesh diagram (140,040 elements). The pumping borehole KAS06 was modelled as a truss element to calculate the velocity distribution along the borehole. Water-conductive zones were modelled as represented in Fig.3.2 based on the conceptual model constructed by Wikberg *et al.* /1991/. One plane corresponds to one water-conductive structure except for EW-5, NE-1a and NE-1b, which have relatively large widths, more than 50 m, and are located near KAS06. The thick structures were modelled with a bundle of planes, four planes for EW-5 and two planes for NE-1a and NE-1b, by considering the mesh size ranging from 10 to 30 m around KAS06 . Therefore the number of planes which correspond to a specific water-conductive structure should be changed depending on the mesh size.

The parameters relating to groundwater flow analysis are listed in Table 3.1. The transmissivities of the fractures were determined according to Wikberg *et al.* /1991/. The fracture width in the calculation was determined from the position of the fracture and the mesh diagram instead of the provisional fracture width of 1 m shown in Table 3.1. The specific storage coefficients of the fractures and a rock matrix were assumed to be 10^{-5} m^{-1} and 10^{-7} m^{-1}, respectively, for analysis of transient groundwater drawdowns.

The contour map of the groundwater level on Aspo island depicted by Svensson /1991a/ was used as an initial condition and a boundary condition of the surface plane. The hydrostatic groundwater pressure distribution was applied to the boundary of the side planes, and an impermeable condition was applied to the boundary of the base plane.

3.2 Tracer migration conditions

The region of the solute migration simulation during the LPT-2 experiment adopted here was extracted from the region of the groundwater flow simulation. The area near KAS06 was taken out and a finer mesh diagram illustrated in Fig.3.3 was remade, since the tracer migration toward the pumping borehole was recognized to be dominant. The simulated results of the steady-state groundwater flow were applied to the tracer migration calculation.

Several tracer injections in 6 sections of 5 boreholes were carried out during the LPT-2 experiment. The pathway from the tracer injection borehole KAS08, section M1 was selected for the tracer migration analysis, because of a relatively short Darcian time from KAS08, M1 to KAS06 according to Svensson /1991b/. The tracer (Rhenium-186) input was provided with the Dirichlet condition at the point of application. The mass release rate of radioactivity used was based on the measured concentration in groundwater samples taken from the injection section /Rhen *et al.*, 1992/.

The parameters relating to tracer migration are listed in Table 3.2. The parameters were obtained by considering the parameters predicted by an one-dimensional convective-dispersive equation along the trajectory from KAS08, M1 /Rhen *et al.*, 1992/.

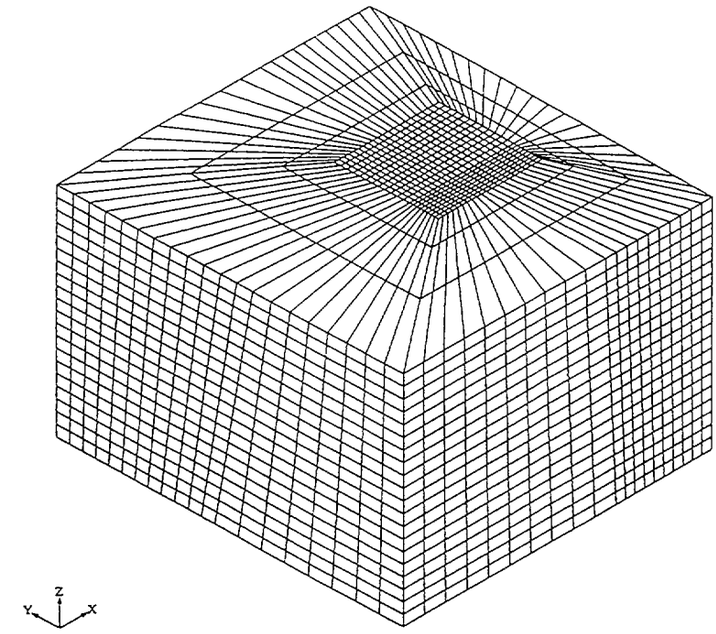

1800m × 2000m × 1300m

Coarse mesh diagram (total elements ; 14,020)

Fig. 3.1(a) Coarse mesh diagram for groundwater flow analysis

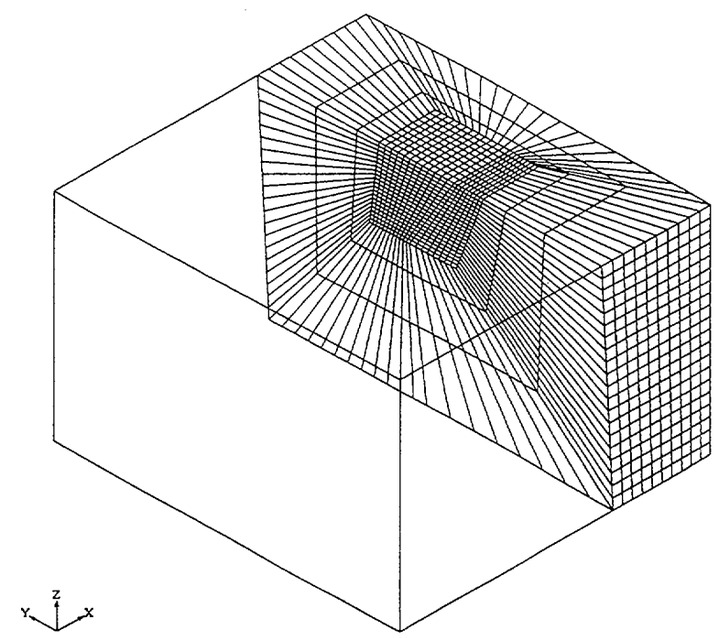

Δ x min = 27.5m

Δ y min = 19.4m

Δ z min = 25.0m

Fig. 3.1(b) Vertical section of coarse mesh diagram

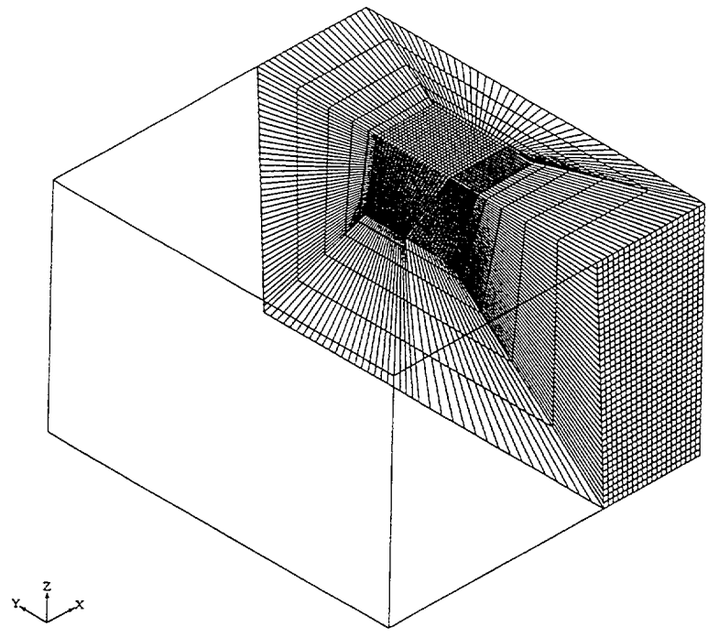

Fine mesh diagram (total elements ; 140,040)

Δ xmin = 13.75m
Δ ymin = 9.7 m
Δ zmin = 12.5 m

Fig. 3.1(c) Vertical section of fine mesh diagram for groundwater flow analysis

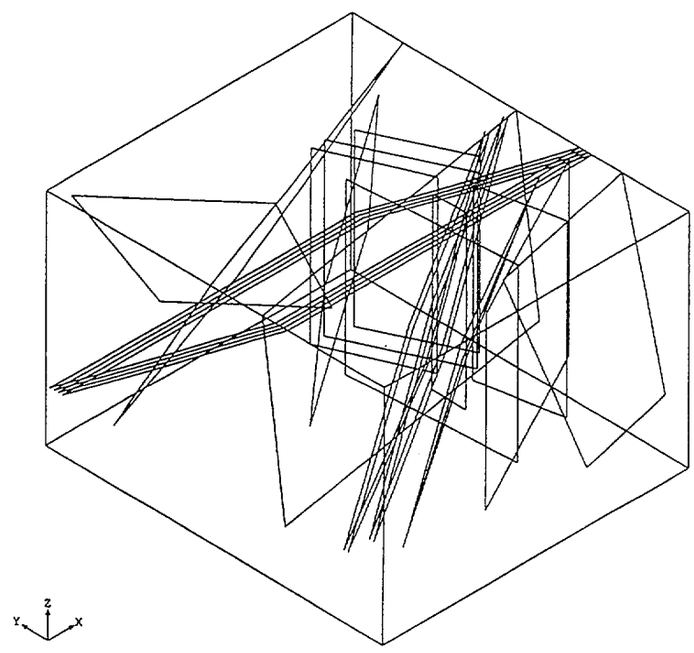

Fig. 3.2 Fracture planes for smeared fracture model

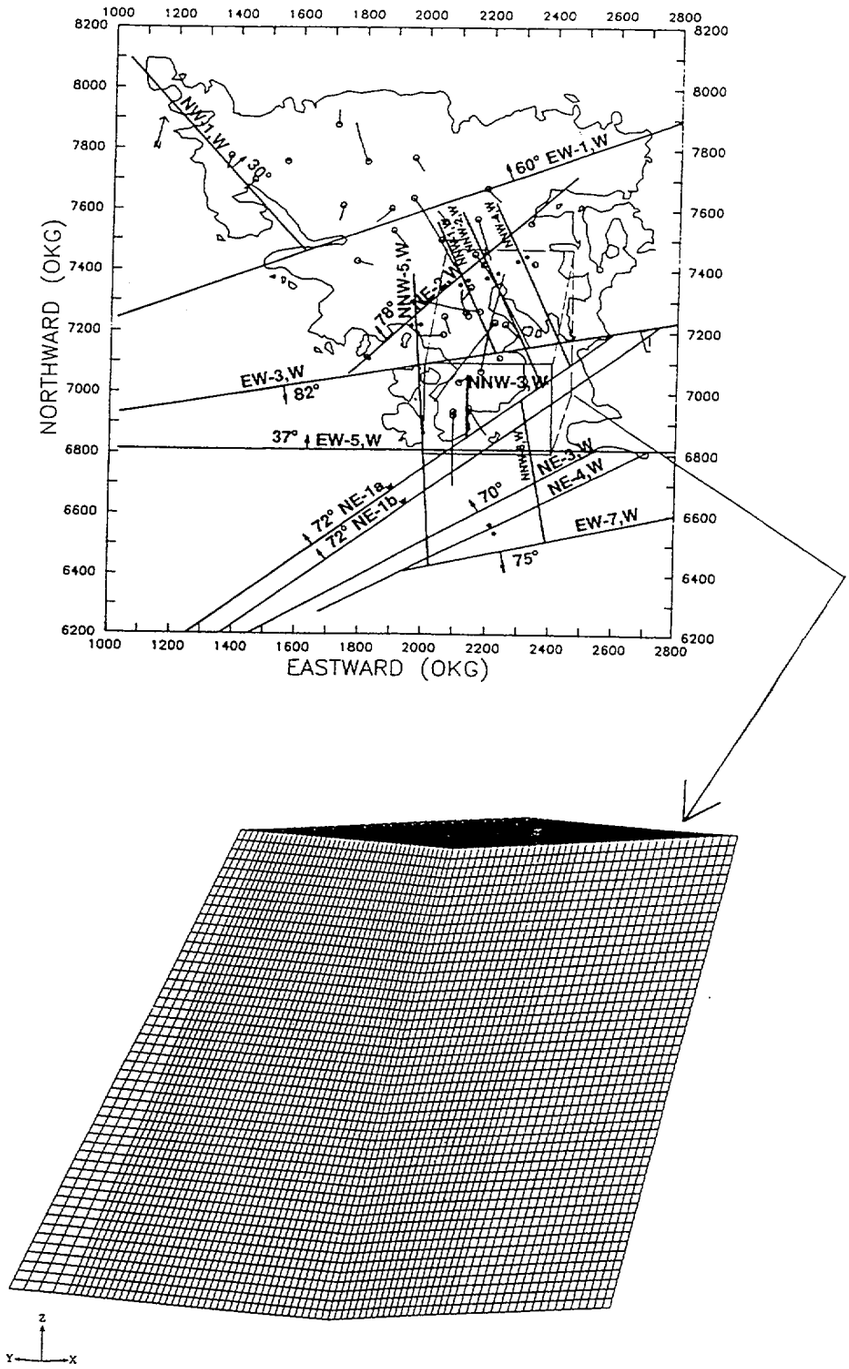

400m × (300～450)m × 500m

Δx ≒ 10m, Δy ≒ (10～13)m, Δz = 10m

total nodes ; 94,095

total elements ; 88,000

Fig. 3.3 Region and mesh diagram for tracer migration analysis

Table 3.1 Input parameters for groundwater flow analysis

Fracture/Matrix	T (m2/s)**	d (m)	N (-)	Width range**
EW-1	2.00E-05	1	1	50-100m
EW-3	5.00E-07	1	1	10-15m
EW-5	2.00E-05	1	4	100m
EW-7	1.40E-04	1	1	10-20m
NE-1a	2.00E-04	1	2	50m
NE-1b	2.00E-04	1	2	50m
NE-2	4.00E-06	1	1	5-10m
NE-3	3.00E-05	1	1	5-10m
NE-4	3.50E-04	1	1	5-10m
NNW-1	1.50E-05	1	1	1-3m
NNW-2	4.00E-05	1	1	1-3m
NNW-3	2.00E-05	1	1	1-3m
NNW-4	4.00E-05	1	1	1-3m
NNW-5	5.00E-05	1	1	1-3m
NNW-6	5.00E-05	1	1	1-3m
NW-1	7.00E-06	1	1	-
Matrix***	-	-	-	-

* T ; transmissivity, d ; fracture width, N ; number of fracture planes
** TR-91-22
***The hydraulic conductivity of the rock matrix is assumed to be 1.0E-10m/s

Table 3.2 Input parameters for tracer migration analysis

Parameters	Fractures	Matrix
aL (m)	20	10
aT (m)	2	0.2
am (m2/s)	0	0
n (-)	0.0005	0.0001
Kd (ml/g)	0	0

* aL ; longitudinal dispersivity, aT ; lateral dispersivity
am ; diffusion coefficient, n ; porosity, Kd ; distribution coefficient

4 SIMULATED RESULTS AND DISCUSSION

4.1 Groundwater flow simulation

A steady-state analysis of groundwater flow with a pumping rate of 2.25 l/s at the borehole KAS06 was carried out. Drawdown is plotted against distance to the relevant sections of the observation boreholes in Figs.4.1 and 4.2. Figure 4.1 compares the calculated drawdowns using a coarse mesh diagram with measured drawdowns. On the other hand, Fig.4.2 compares the calculated drawdowns using a fine mesh diagram with measured drawdowns. Tables 4.1 and 4.2 list the differences between the calculated groundwater drawdowns and the measured ones, and the relative differences. The simulated steady-state groundwater drawdowns agreed fairly well with the measured groundwater drawdowns irrespective of the distance from the point of application of KAS06, although considerable discrepancies were found in several sections. In addition, the simulated results were not greatly dependent upon the number of finite-element meshes, as can be seen by comparing Figs.4.1 and 4.2. This suggests that the smeared fracture model is effective when simulating an approximate groundwater flow through fractured media, since it is not necessary to make an enormous number of finite-element meshes.

Representative trajectories to KAS06 obtained from steady-state calculation using the fine mesh diagram are depicted in Fig.4.3. Several starting positions within the same borehole section were selected for trajectory calculation. It is clear that groundwater particles with different starting positions flow through a similar pathway if the positions are in the same section. Table 4.3 lists Darcian travel times from injection boreholes to KAS06, compared with the results calculated by Svensson /1991b/. The travel times calculated by FEGM agreed fairly well with the results derived by Svensson, irrespective of the mesh diagrams.

The calculated velocity distribution of groundwater flow along the pumping borehole KAS06 is illustrated in Fig.4.4. Velocity increased with decreasing depth, due to an increasing inflow of groundwater to KAS06 through fractures. A sudden change in velocity at 100 m distant from the ground surface is due to the increase in diameter of the shallower part of the borehole.

The calculated groundwater flow and the flow rates measured by a dilution method during the LPT-2 experiment are compared in Table 4.4. The calculated flow rates were much lower than the measured values. The difference may be due to the characteristic of the smeared fracture model that the calculated groundwater flow represents the average value within the element, including both fractures and a matrix.

The simulated results of unsteady-state groundwater flow are shown in Fig.4.5, together with the measured transient drawdowns. In some sections the calculated transient drawdown and the measured drawdown agreed, while in other sections they did not agree, since the specific storage coefficient for all the fractures was fixed at 10^{-5} m^{-1}. A more appropriate specific storage coefficient can be identified for each fracture by fitting the calculated transient drawdowns to the measured ones more closely. In addition, the calculated transient drawdowns were dependent on the mesh size, although the calculated steady-state drawdowns were not greatly dependent on the mesh size, as described above. The more finely the meshes were divided, the earlier the drawdowns responded. This stems from a high dependency of the storage coefficient, derived from the volume-weighted value of the fractures and the matrix within the element, on mesh size.

4.2 Tracer migration simulation

The transient analysis of the tracer migration was conducted assuming that a steady-state groundwater flow induced by a constant pumping rate of 2.25 l/min at KAS06 prevailed. The injection of radioactivity at KAS08, M1 was based on the experimental conditions. The simulated results of the groundwater flow indicate that several fractures are involved in the tracer migration from KAS08, M1 to KAS06. Figure 4.6 illustrates a three-dimensional concentration contour of Rhenium-186 used as a tracer at t = 252 h. It is apparent that the injected tracer migrates along the trajectories shown in Fig.4.3.

The breakthrough curve of Re-186 at a sampling level of 190 m of KAS06 is represented in Fig.4.7. The calculated breakthrough curve agreed with the observed data, assuming that the recovery ratio of Re-186 was 10%. The calculated breakthrough curve of Re-186 at a sampling level of 340 m also agreed with the observed data, as shown in Fig.4.8. The agreement between these two breakthrough curves indicates that a part of the injected tracer migrated through the simulated pathway. It is supposed that there are more water-conductive pathways intersecting KAS08, KAS06, and/or the related fractures than first considered based on such a low tracer recovery.

Similarly, the breakthrough of uranine from the borehole KAS05 section M3 was calculated. In this calculation the porosity of fractures was changed to 0.00025 because the peak concentration of uranine breakthrough was not available in case of the fracture porosity of 0.0005 shown in Table 3.1. Figure 4.9 compares the calculated and observed breakthrough of uranine from KAS05 at a sampling level of 390 m in KAS06. The first high peak of the observed breakthrough is recognized from the borehole KAS12 and the second low peak is from KAS05, according to Rhen *et al.*/1992/. The calculated breakthrough of uranine followed the observed one even if the fracture porosity was reduced to 0.00025 and the

recovery ratio of uranine was assumed to be 100%. This suggests that the breakthrough of uranine at KAS06 should have been monitored for longer period.

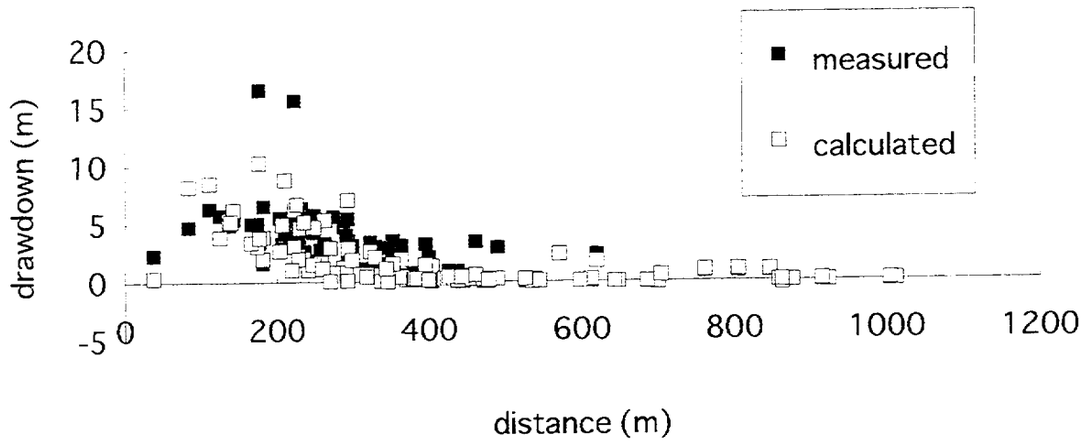

Fig. 4.1 Calculated drawdowns from steady-state analysis using coarse mesh diagram compared with measured drawdowns

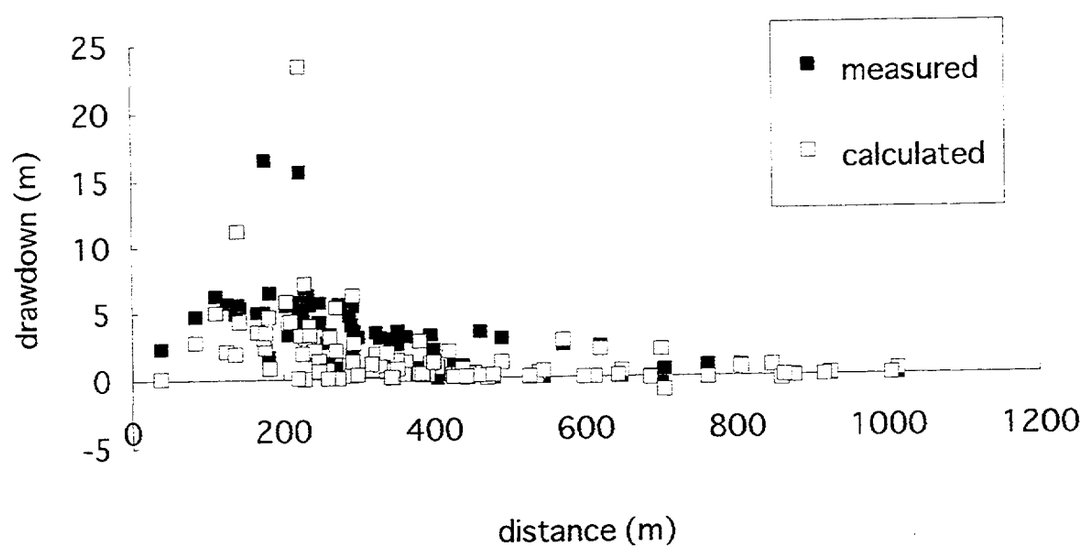

Fig. 4.2 Calculated drawdowns from steady-state analysis using fine mesh diagram compared with measured drawdowns

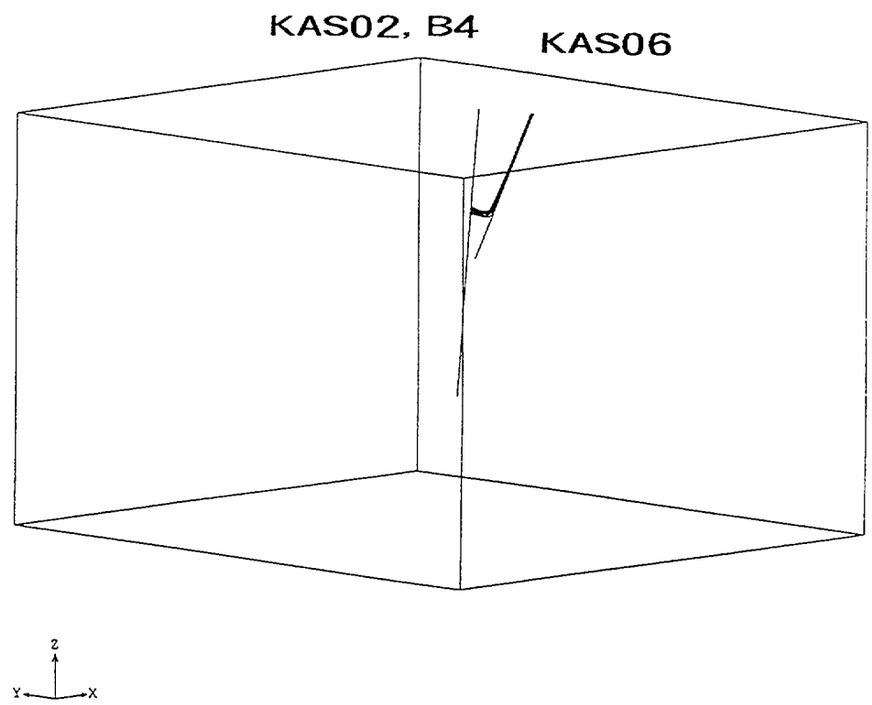

Fig. 4.3 (a) Trajectories from KAS02, B4 to KAS06 from steady-state analysis using fine mesh diagram

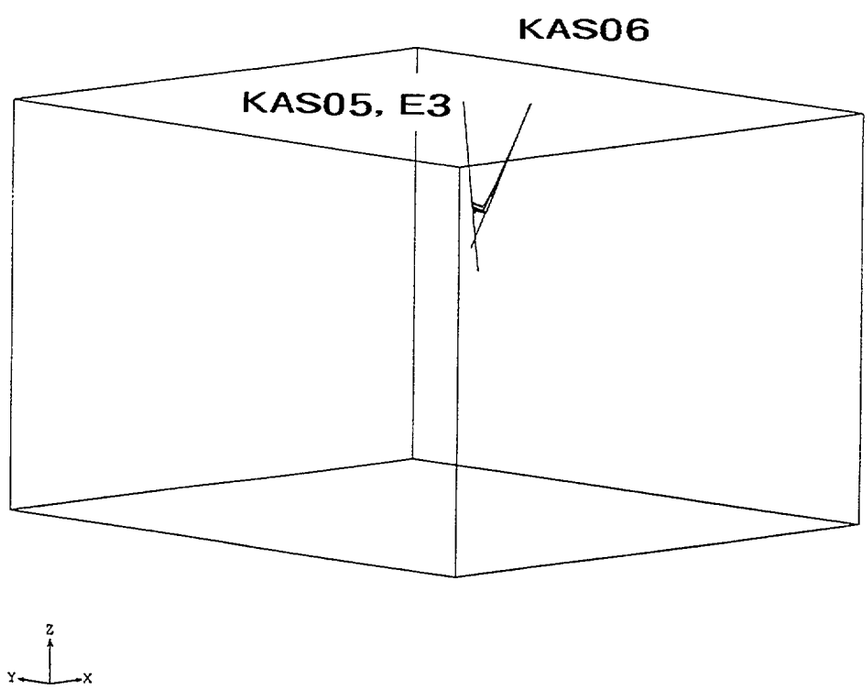

Fig. 4.3 (b) Trajectories from KAS05, E3 to KAS06 form steady-state analysis using fine mesh diagram

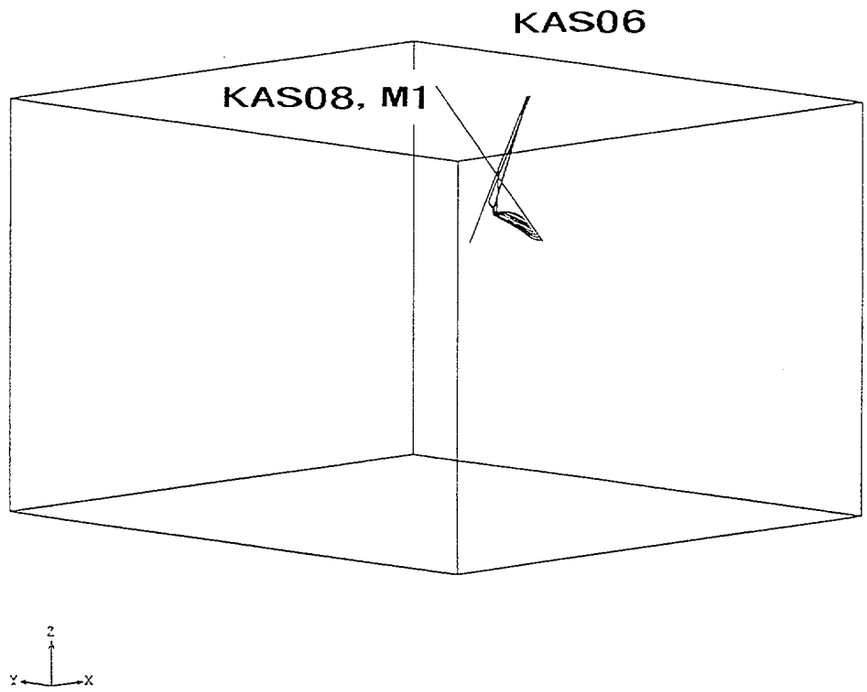

Fig. 4.3 (c) Trajectories from KAS08, M1 to KAS06 from steady-state analysis using fine mesh diagram

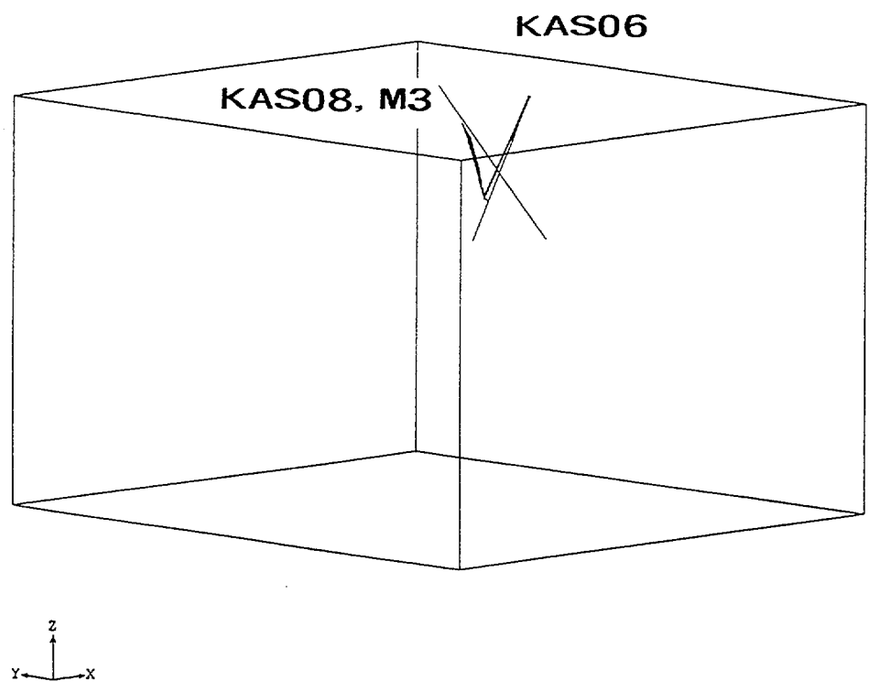

Fig. 4.3 (d) Trajectories from KAS08, M3 to KAS06 from steady-state analysis using fine mesh diagram

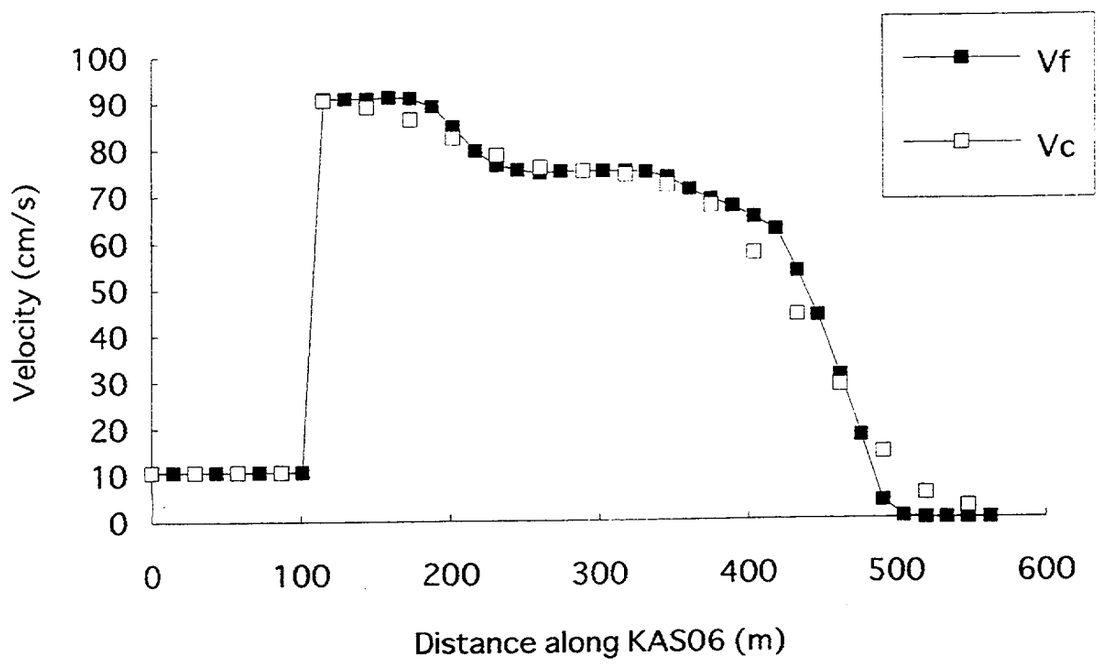

Fig. 4.4 Calculated velocity distribution of groundwater flow along KAS06 (Vf : flow velocity for fine mesh, Vc : flow velocity for coarse mesh)

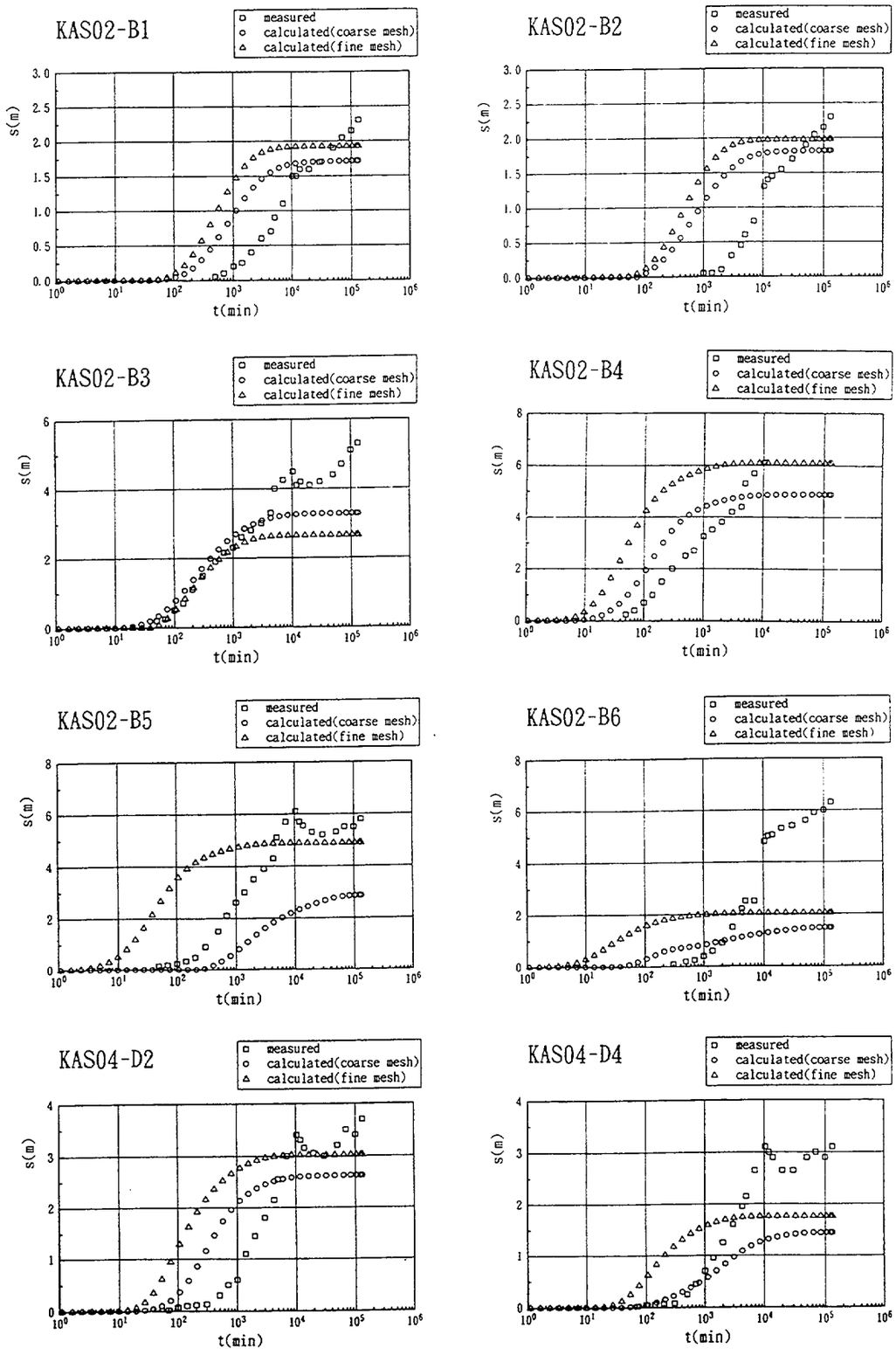

Fig. 4.5 (a) Calculated and measured drawdowns with time for KAS02 and KAS04

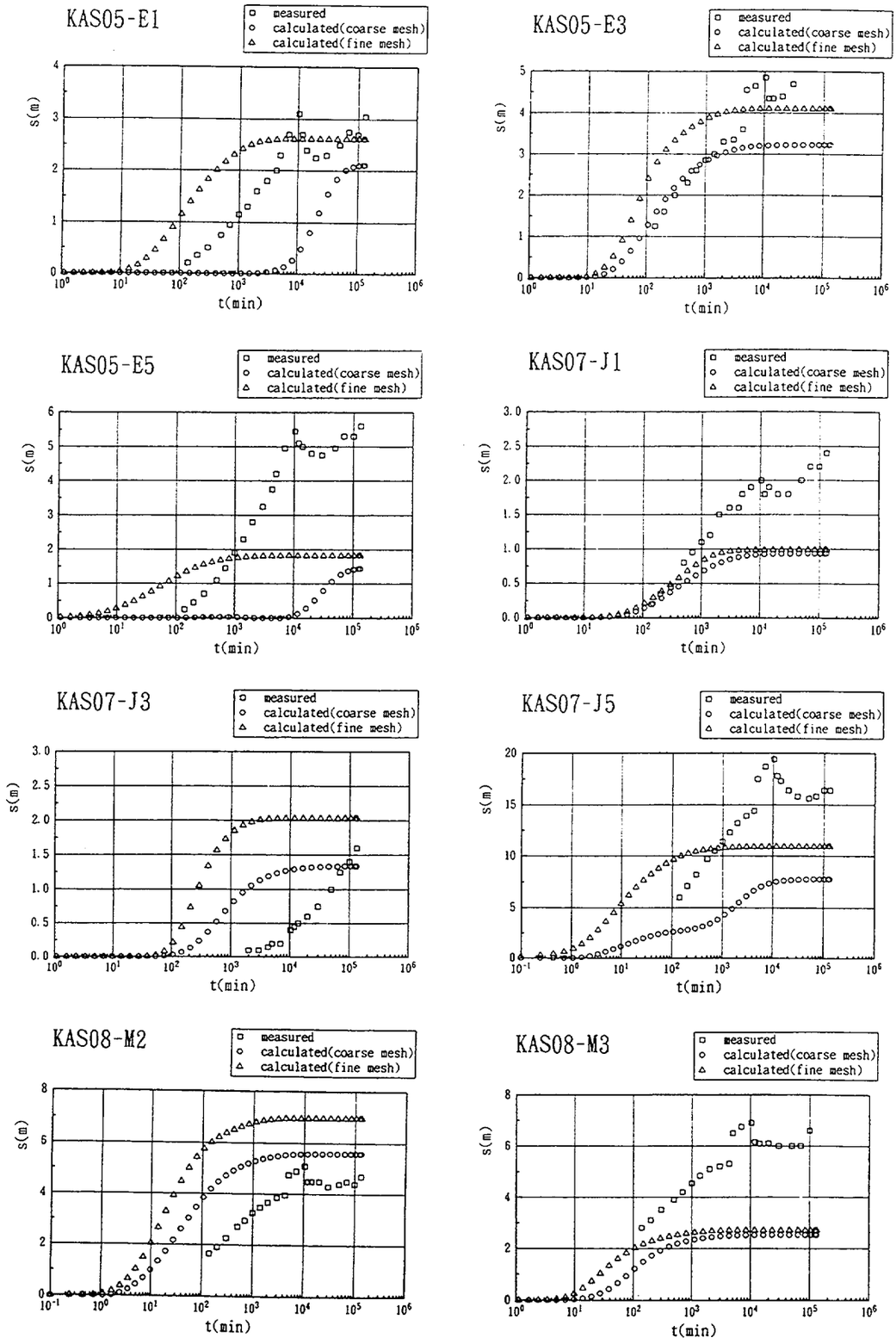

Fig. 4.5 (b) Calculated and measured drawdowns with time for KAS05, KAS07 and KAS08

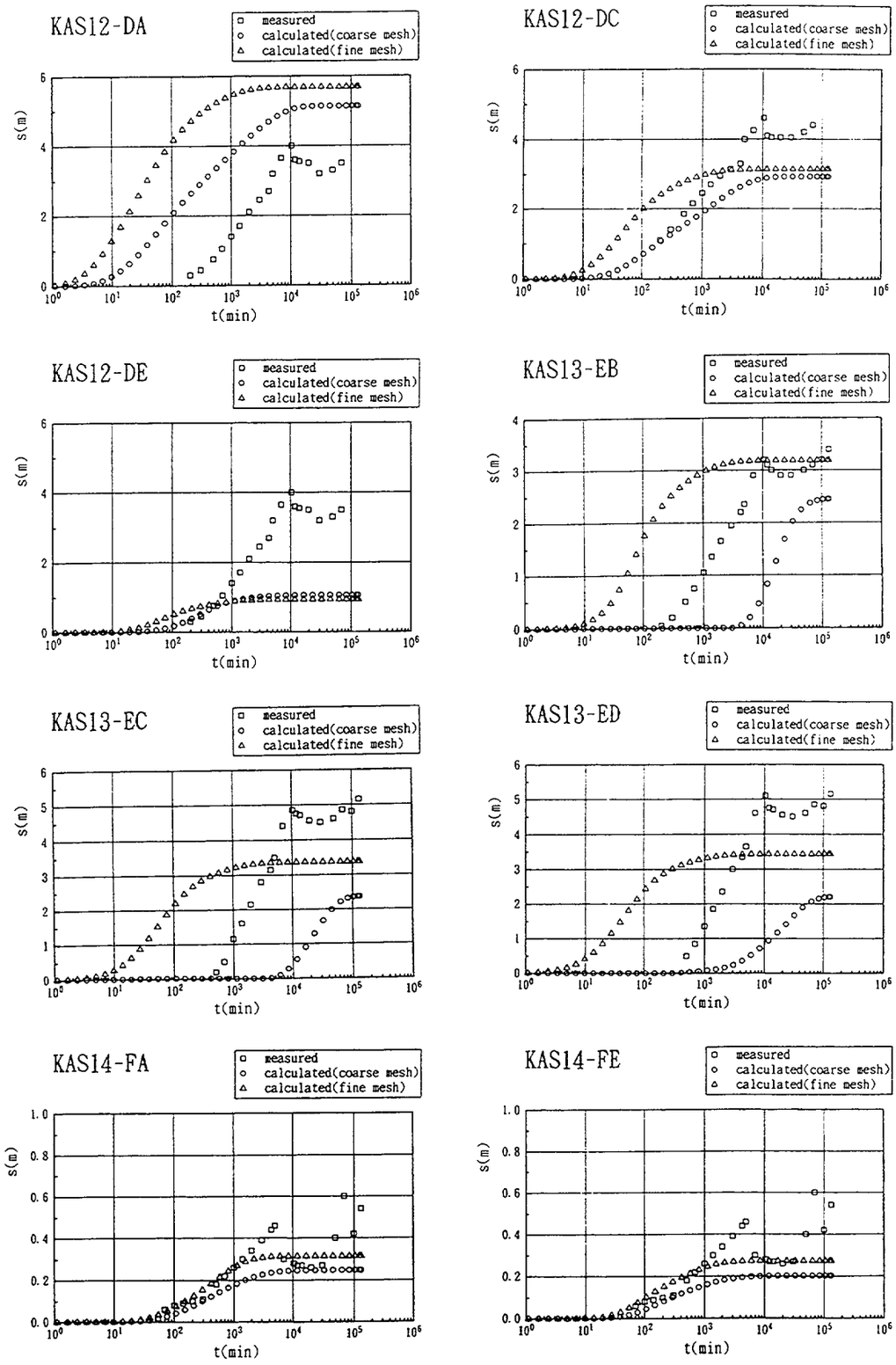

Fig. 4.5 (c) Calculated and measured drawdowns with time for KAS12, KAS13 and KAS14

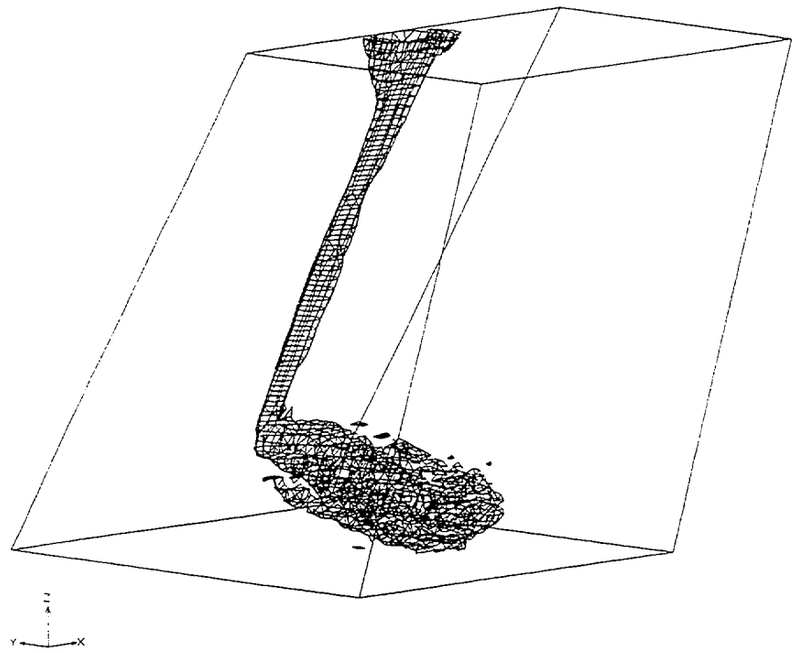

Fig. 4.6(a) Calculated three-dimensional concentration contour of Rhenium-186 at t = 252 hrs (C = 0.5 kBq/l)

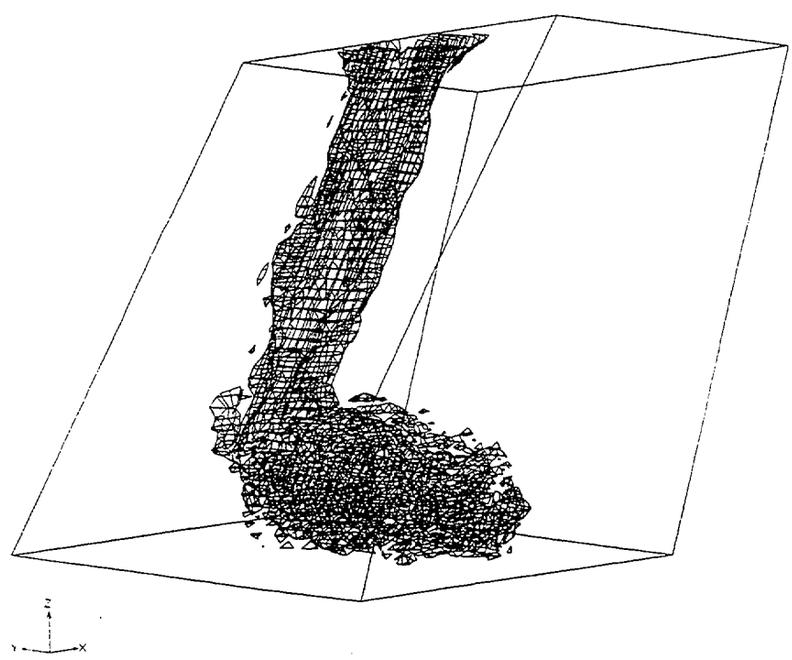

Fig. 4.6(b) Calculated three-dimensional concentration contour of Rhenium-186 at t = 252 hrs (C = 0.01 kBq/l)

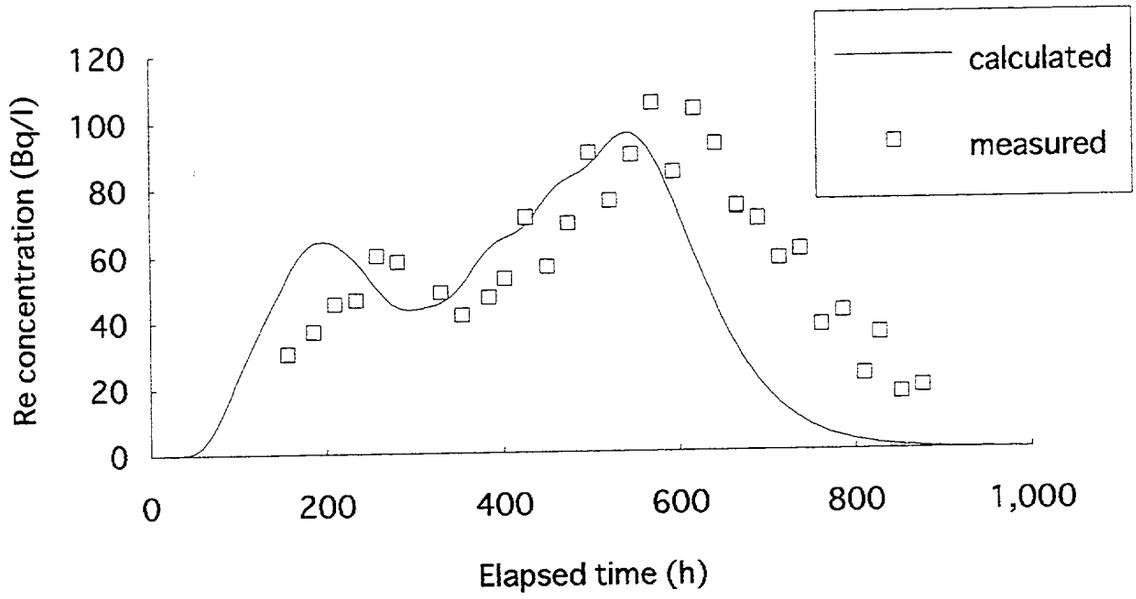

Fig. 4.7 Calculated breakthrough curve corrected for recovery of Rhenium-186 and measured breakthrough curve at sampling level 190m in KAS06

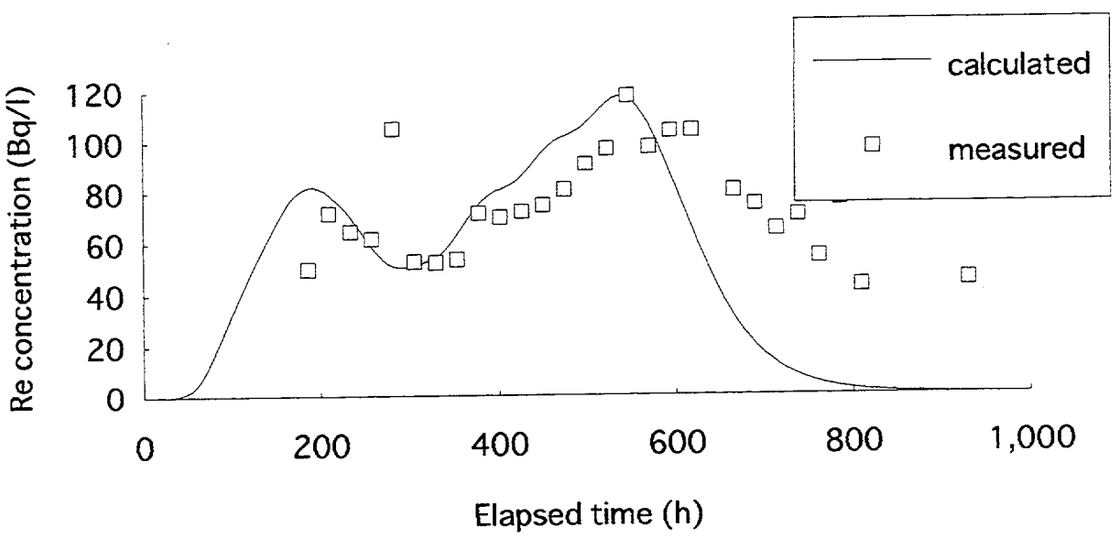

Fig. 4.8 Calculated breakthrough curve corrected for recovery of Rhenium-186 and measured breakthrough curve at sampling level 340m in KAS06

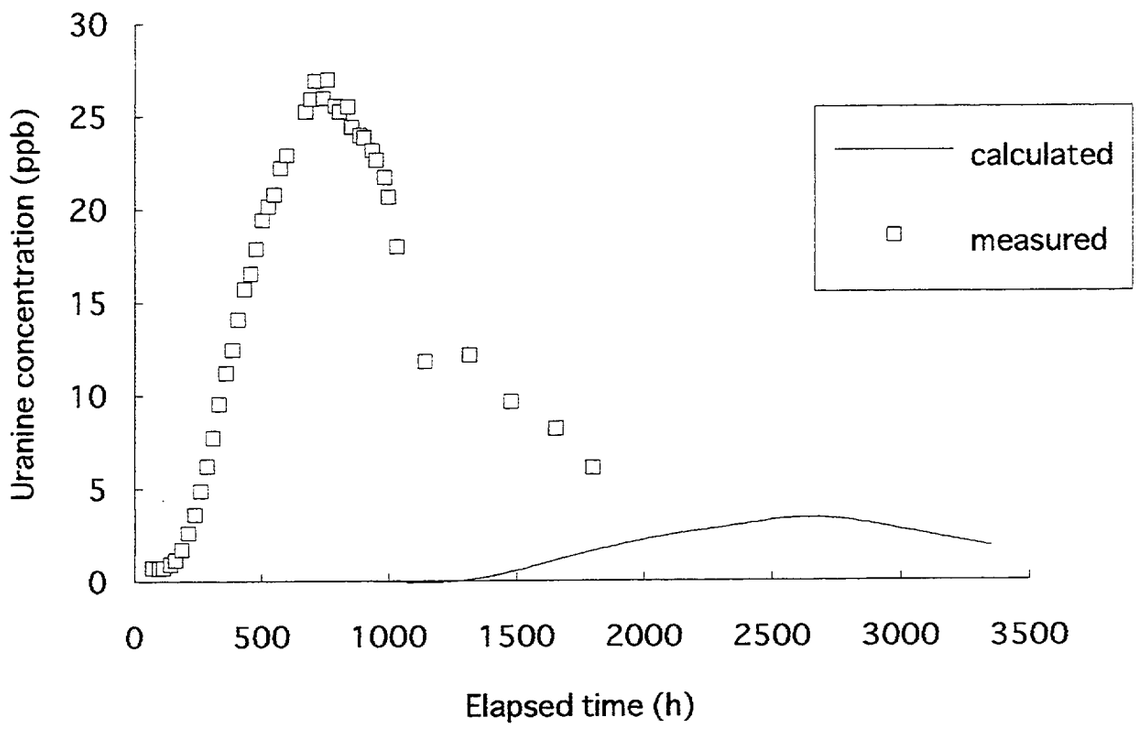

Fig. 4.9 Calculated and measured breakthrough curve of uranine at sampling level 390m in KAS06

Table 4.1 List of calculated drawdowns for coarse mesh

Borehole	Depth (m)	Section	Distance(m)	Measured(m)	Calculated(m)	Difference(m)	Relative-diff.
KAS01	0-101	A1	229	6.2	1.84	4.36	0.7
KAS02	0-113	B6	233	6.3	1.53	4.77	0.76
KAS02	114-308	B5	125	5.7	2.96	2.74	0.48
KAS02	309-345	B4	111	6.3	5.06	1.24	0.2
KAS02	346-799	B3	293	5.4	3.4	2	0.37
KAS02	800-854	B2	571	2.4	1.89	0.51	0.21
KAS02	855-924	B1	619	2.3	1.78	0.52	0.23
KAS03	0-106	C6	700	0	-0.03	0.03	#DIV/0!
KAS03	107-252	C5	686	0	0.1	-0.1	#DIV/0!
KAS03	253-376	C4	704	0.5	0.46	0.04	0.08
KAS03	377-532	C3	761	0.8	0.82	-0.02	0.02
KAS03	533-626	C2	805	0.8	0.91	-0.11	0.14
KAS03	627-1002	C1	846	0.8	0.94	-0.14	0.18
KAS04	0-185	D6	404	0	1.08	-1.08	#DIV/0!
KAS04	186-214	D5	395	3.2	1.19	2.01	0.63
KAS04	215-287	D4	363	3.1	1.49	1.61	0.52
KAS04	288-331	D3	323	3.4	2.28	1.12	0.33
KAS04	332-392	D2	294	3.5	2.72	0.78	0.22
KAS04	393-481	D1	262	3.3	3.42	-0.12	0.04
KAS05	0-171	E5	235	5.5	1.5	4	0.73
KAS05	172-319	E4	137	4.9	3.44	1.46	0.3
KAS05	520-380	E3	142	5.4	3.34	2.06	0.38
KAS05	381-439	E2	207	3.3	2.5	0.8	0.24
KAS05	440-550	E1	230	3	2.19	0.81	0.27
KAS07	0-109	J6	223	15.6	2.31	13.29	0.85
KAS07	110-190	J5	176	16.5	8.05	8.45	0.51
KAS07	191-290	J4	139	5.6	3.67	1.93	0.34
KAS07	291-410	J3	181	1.6	1.39	0.21	0.13
KAS07	411-500	J2	242	1.8	1.07	0.73	0.41
KAS07	501-604	J1	351	2.5	0.97	1.53	0.61
KAS08	0-139	M4	288	4.7	0.81	3.89	0.83
KAS08	140-200	M3	182	6.5	2.61	3.89	0.6
KAS08	201-502	M2	84	4.7	5.78	-1.08	0.23
KAS08	503-691	M1	229	3.7	1.53	2.17	0.59
KAS09	0-115	AE	420	0.2	0.23	-0.03	0.15
KAS09	116-150	AD	424	0.3	0.25	0.05	0.17
KAS09	151-240	AC	433	0.4	0.26	0.14	0.35
KAS09	241-260	AB	454	0.4	0.27	0.13	0.33
KAS09	261-450	AA	539	0.2	0.25	-0.05	0.25
KAS10	0-100	BA	370	0.6	0.17	0.43	0.72
KAS11	0-46	CF	391	0.4	0.15	0.25	0.63
KAS11	47-64	CE	385	0.5	0.19	0.31	0.62
KAS11	65-115	CD	365	0.5	0.34	0.16	0.32
KAS11	116-152	CC	344	0.6	0.45	0.15	0.25
KAS11	153-183	CB	333	0.9	0.51	0.39	0.43
KAS11	184-249	CA	319	0.5	0.58	-0.08	0.16
KAS12	0-101	DE	352	3.5	1.09	2.41	0.69
KAS12	102-233	DD	329	3	1.48	1.52	0.51
KAS12	234-277	DC	248	4.2	3.03	1.17	0.28
KAS12	278-329	DB	223	5.8	3.87	1.93	0.33
KAS12	330-380	DA	210	4.1	5.32	-1.22	0.3
KAS13	0-150	EE	204	5.5	2.02	3.48	0.63
KAS13	151-190	ED	174	5	2.29	2.71	0.54
KAS13	191-220	EC	166	5	2.46	2.54	0.51
KAS13	221-330	EB	177	3.4	2.54	0.86	0.25
KAS13	331-407	EA	236	2.6	2.27	0.33	0.13
KAS14	0-130	FE	381	0.6	0.21	0.39	0.65
KAS14	131-138	FD	379	0.7	0.25	0.45	0.64
KAS14	139-146	FC	380	0.7	0.26	0.44	0.63
KAS14	147-175	FB	381	0.6	0.26	0.34	0.57
KAS14	175-212	FA	384	0.6	0.26	0.34	0.57

HAS01	0-100	G1	445	0	0.33	-0.33	#DIV/0!
HAS02	0-72	H2	1013	0	0.04	-0.04	#DIV/0!
HAS02	73-93	H1	1005	0	0.06	-0.06	#DIV/0!
HAS03	0-50	I2	535	0	0	0	#DIV/0!
HAS03	51-100	I1	471	0	0.14	-0.14	#DIV/0!
HAS04	0-100	K2	291	4	0.63	3.37	0.84
HAS04	101-201	K1	258	2.7	1.08	1.62	0.6
HAS05	0-15	L3	293	1.8	0.07	1.73	0.96
HAS05	16-40	L2	274	5.6	0.54	5.06	0.9
HAS05	41-100	L1	248	5.7	1.15	4.55	0.8
HAS06	0-40	N2	338	1.5	0.07	1.43	0.95
HAS06	41-100	N1	38	2.3	0.48	1.82	0.79
HAS07	0-40	O2	438	0.9	0.08	0.82	0.91
HAS07	41-100	O1	426	0.9	0.44	0.46	0.51
HAS08	0-65	P2	648	0	0.01	-0.01	#DIV/0!
HAS08	66-125	P1	612	0	0.14	-0.14	#DIV/0!
HAS09	0-10	Q2	643	0	0	0	#DIV/0!
HAS09	11-125	Q1	598	0	0.07	-0.07	#DIV/0!
HAS10	0-10	R2	858	0	-0.01	0.01	#DIV/0!
HAS10	11-125	R1	863	0	-0.11	0.11	#DIV/0!
HAS11	0-30	S2	876	0	0	0	#DIV/0!
HAS11	31-125	S1	862	0	0.03	-0.03	#DIV/0!
HAS12	0-60	T2	924	0	0.01	-0.01	#DIV/0!
HAS12	61-125	T1	915	0	0.08	-0.08	#DIV/0!
HAS13	0-50	U2	346	0.5	0.02	0.48	0.96
HAS13	51-100	U1	260	1.1	0.87	0.23	0.21
HAS14	0-50	V2	270	0	2.2	-2.2	#DIV/0!
HAS14	51-100	V1	226	4.6	5.28	-0.68	0.15
HAS15	0-40	X2	270	0.8	0.03	0.77	0.96
HAS15	41-120	X1	220	5.2	0.74	4.46	0.86
HAS16	0-40	Y2	318	1.1	0.3	0.8	0.73
HAS16	41-120	Y1	299	3.1	1.24	1.86	0.6
HAS17	0-40	Z2	399	2.1	0.11	1.99	0.95
HAS17	41-120	Z1	344	2.9	0.78	2.12	0.73
HAS18	0-35	PB	489	2.9	0.17	2.73	0.94
HAS18	36-150	PA	461	3.4	0.44	2.96	0.87
HAS19	0-35	QB	545	0	0.05	-0.05	#DIV/0!
HAS19	36-150	QA	526	0	0.17	-0.17	#DIV/0!
HAS20	0-35	RB	478	0	0.11	-0.11	#DIV/0!
HAS20	36-150	RA	443	0	0.27	-0.27	#DIV/0!

Table 4.2 List of calculated drawdowns for fine mesh

Borehole	Depth (m)	Section	Distance(m)	Measured(m)	Calculated(m)	Difference(m)	Relative-diff.
KAS01	0-101	A1	229	6.2	0	6.2	1
KAS02	0-113	B6	233	6.3	2.41	3.89	0.62
KAS02	114-308	B5	125	5.7	2.09	3.61	0.63
KAS02	309-345	B4	111	6.3	5.01	1.29	0.2
KAS02	346-799	B3	293	5.4	6.25	-0.85	0.16
KAS02	800-854	B2	571	2.4	2.72	-0.32	0.13
KAS02	855-924	B1	619	2.3	2.03	0.27	0.12
KAS03	0-106	C6	700	0	1.97	-1.97	#DIV/0!
KAS03	107-252	C5	686	0	-0.11	0.11	#DIV/0!
KAS03	253-376	C4	704	0.5	-1.01	1.51	3.02
KAS03	377-532	C3	761	0.8	-0.12	0.92	1.15
KAS03	533-626	C2	805	0.8	0.6	0.2	0.25
KAS03	627-1002	C1	846	0.8	0.74	0.06	0.08
KAS04	0-185	D6	404	0	0.79	-0.79	#DIV/0!
KAS04	186-214	D5	395	3.2	1.07	2.13	0.67
KAS04	215-287	D4	363	3.1	1.19	1.91	0.62
KAS04	288-331	D3	323	3.4	1.8	1.6	0.47
KAS04	332-392	D2	294	3.5	2.62	0.88	0.25
KAS04	393-481	D1	262	3.3	3.09	0.21	0.06
KAS05	0-171	E5	235	5.5	3.93	1.57	0.29
KAS05	172-319	E4	137	4.9	1.87	3.03	0.62
KAS05	520-380	E3	142	5.4	4.28	1.12	0.21
KAS05	381-439	E2	207	3.3	4.21	-0.91	0.28
KAS05	440-550	E1	230	3	3.06	-0.06	0.02
KAS07	0-109	J6	223	15.6	23.39	-7.79	0.5
KAS07	110-190	J5	176	16.5	2.28	14.22	0.86
KAS07	191-290	J4	139	5.6	11.18	-5.58	1
KAS07	291-410	J3	181	1.6	4.63	-3.03	1.89
KAS07	411-500	J2	242	1.8	2.08	-0.28	0.16
KAS07	501-604	J1	351	2.5	1.31	1.19	0.48
KAS08	0-139	M4	288	4.7	1.02	3.68	0.78
KAS08	140-200	M3	182	6.5	0.81	5.69	0.88
KAS08	201-502	M2	84	4.7	2.77	1.93	0.41
KAS08	503-691	M1	229	3.7	7.14	-3.44	0.93
KAS09	0-115	AE	420	0.2	1.97	-1.77	8.85
KAS09	116-150	AD	424	0.3	0.26	0.04	0.13
KAS09	151-240	AC	433	0.4	0.3	0.1	0.25
KAS09	241-260	AB	454	0.4	0.34	0.06	0.15
KAS09	261-450	AA	539	0.2	0.35	-0.15	0.75
KAS10	0-100	BA	370	0.6	0.27	0.33	0.55
KAS11	0-46	CF	391	0.4	0.26	0.14	0.35
KAS11	47-64	CE	385	0.5	0.21	0.29	0.58
KAS11	65-115	CD	365	0.5	0.27	0.23	0.46
KAS11	116-152	CC	344	0.6	0.46	0.14	0.23
KAS11	153-183	CB	333	0.9	0.57	0.33	0.37
KAS11	184-249	CA	319	0.5	0.61	-0.11	0.22
KAS12	0-101	DE	352	3.5	0.67	2.83	0.81
KAS12	102-233	DD	329	3	0.96	2.04	0.68
KAS12	234-277	DC	248	4.2	1.32	2.88	0.69
KAS12	278-329	DB	223	5.8	3.22	2.58	0.44
KAS12	330-380	DA	210	4.1	4.28	-0.18	0.04
KAS13	0-150	EE	204	5.5	5.82	-0.32	0.06
KAS13	151-190	ED	174	5	3.04	1.96	0.39
KAS13	191-220	EC	166	5	3.52	1.48	0.3
KAS13	221-330	EB	177	3.4	3.46	-0.06	0.02
KAS13	331-407	EA	236	2.6	3.27	-0.67	0.26
KAS14	0-130	FE	381	0.6	2.73	-2.13	3.55
KAS14	131-138	FD	379	0.7	0.28	0.42	0.6
KAS14	139-146	FC	380	0.7	0.31	0.39	0.56
KAS14	147-175	FB	381	0.6	0.32	0.28	0.47
KAS14	175-212	FA	384	0.6	0.32	0.28	0.47

HAS01	0-100	G1	445	0	0.32	-0.32	#DIV/0!
HAS02	0-72	H2	1013	0	0.35	-0.35	#DIV/0!
HAS02	73-93	H1	1005	0	0.04	-0.04	#DIV/0!
HAS03	0-50	I2	535	0	0.04	-0.04	#DIV/0!
HAS03	51-100	I1	471	0	0.01	-0.01	#DIV/0!
HAS04	0-100	K2	291	4	0.21	3.79	0.95
HAS04	101-201	K1	258	2.7	0.66	2.04	0.76
HAS05	0-15	L3	293	1.8	1.25	0.55	0.31
HAS05	16-40	L2	274	5.6	0.02	5.58	1
HAS05	41-100	L1	248	5.7	0.58	5.12	0.9
HAS06	0-40	N2	338	1.5	1.85	-0.35	0.23
HAS06	41-100	N1	38	2.3	0.12	2.18	0.95
HAS07	0-40	O2	438	0.9	0.65	0.25	0.28
HAS07	41-100	O1	426	0.9	0.07	0.83	0.92
HAS08	0-65	P2	648	0	0.44	-0.44	#DIV/0!
HAS08	66-125	P1	612	0	0.01	-0.01	#DIV/0!
HAS09	0-10	Q2	643	0	0.11	-0.11	#DIV/0!
HAS09	11-125	Q1	598	0	-0.01	0.01	#DIV/0!
HAS10	0-10	R2	858	0	-0.26	0.26	#DIV/0!
HAS10	11-125	R1	863	0	0	0	#DIV/0!
HAS11	0-30	S2	876	0	-0.06	0.06	#DIV/0!
HAS11	31-125	S1	862	0	0.01	-0.01	#DIV/0!
HAS12	0-60	T2	924	0	0.1	-0.1	#DIV/0!
HAS12	61-125	T1	915	0	0	0	#DIV/0!
HAS13	0-50	U2	346	0.5	0.04	0.46	0.92
HAS13	51-100	U1	260	1.1	0.02	1.08	0.98
HAS14	0-50	V2	270	0	2.1	-2.1	#DIV/0!
HAS14	51-100	V1	226	4.6	1.87	2.73	0.59
HAS15	0-40	X2	270	0.8	5.32	-4.52	5.65
HAS15	41-120	X1	220	5.2	0.07	5.13	0.99
HAS16	0-40	Y2	318	1.1	1.06	0.04	0.04
HAS16	41-120	Y1	299	3.1	0.3	2.8	0.9
HAS17	0-40	Z2	399	2.1	1.15	0.95	0.45
HAS17	41-120	Z1	344	2.9	0.08	2.82	0.97
HAS18	0-35	PB	489	2.9	1.12	1.78	0.61
HAS18	36-150	PA	461	3.4	0.16	3.24	0.95
HAS19	0-35	QB	545	0	0.48	-0.48	#DIV/0!
HAS19	36-150	QA	526	0	0.06	-0.06	#DIV/0!
HAS20	0-35	RB	478	0	0.21	-0.21	#DIV/0!
HAS20	36-150	RA	443	0	0.12	-0.12	#DIV/0!

Table 4.3 Simulated results of travel times (Darcian times)

Injection hole	Section (m)	Tc (×E+10 s)	Tf (×E+10 s)	Ts (×E+10s)
KAS02	B4	0.6	0.51	0.68
KAS04	D2	4.2	3.12	11.5
KAS05	E3	1.56	1.44	1.1
KAS07	J4	1.5	1.2	0.41
KAS08	M3	0.36	0.66	0.2
KAS08	M1	0.96	0.21	0.16
KAS11	CE	8.4	10.8	3.5
KAS12	DD	2.4	3.48	0.53

* Tc ; travel time for coarse mesh, Tf ; travel time for fine mesh
Ts ; travel time calculated by Svensson (PR25-91-17)

Table 4.4 Comparison between calculated flow rates and measured ones

Borehole	Section	Qc (ml/min)	Qf (ml/min)	Qm (ml/min)
KAS02	B4	0.79	0.86	2
KAS02	B2	0.06	0.06	4
KAS05	E3	0.68	0.65	9
KAS05	E1	0.2	0.01	11
KAS07	J4	1.61	1.32	18
KAS08	M3	1.05	1.12	21
KAS08	M1	3.49	5.89	48
KAS12	DB	0.41	0.19	107
KAS13	EC	0.47	0.07	3.3
KAS14	FB	0.15	0.04	11

* Qc ; calculated flow rate for coarse mesh
Qf : calculated flow rate for fine mesh
Qm : measured flow rate by dilution method

5 SUMMARIES

A three-dimensional smeared fracture model coupled with a groundwater flow simulation code FEGM and a solute migration simulation code FERM was applied to groundwater flow and tracer migration during the LPT-2 experiment. The entire island of Aspo was included in the region for groundwater flow analysis, while the area in the vicinity of the pumping borehole KAS06 was taken out for tracer migration analysis.

The simulated results of the steady-state groundwater flow agreed fairly well with the measured drawdowns, although considerable discrepancies in drawdown were found in several sections. Furthermore, the simulated results were not greatly dependent upon the total number of finite elements. This indicates that the smeared fracture model is effective, since the use of an enormous number of finite-element meshes is not needed when simulating an approximate groundwater flow through fractured media. The considerable disagreement found in several sections may be due to differences in connectivity between the smeared fracture network used here and the real fracture network. The simulated results of the unsteady-state groundwater flow were largely dependent on the specific storage coefficients of the fractures. It is possible to evaluate the specific storage coefficient of each fracture by fitting the simulated drawdown curves to the observed ones more closely.

A particle pathway from KAS08, M1 to KAS06 was selected for tracer migration analysis because of a relatively short Darcian time. The calculated trajectories indicate that several fractures may be involved in the pathway. The simulated concentration of the tracer, Rhenium-186, in the groundwater of KAS06 was in good agreement with the observed one, assuming that the tracer recovery ratio was 10%. This suggests that more water-conductive pathways than first considered reduce the recovery of the injected tracer.

REFERENCES

Kawanishi M, Igarashi T, Mahara Y, Komada H, Maki Y, 1987, Computer models for safety assessment on land disposal of low level wastes. Waste Management '87, 3, Tucson, Arizona, pp 175-180.

Kawanishi M, Tanaka Y, Igarashi T, 1994, Development of performance assessment method on natural barrier system for geological disposal of high-level radioactive wastes (I). CRIEPI Report U93054 (in Japanese).

Rhen I, Svensson U, Andersson J E , Andersson P, Eriksson C O, Gustafsson E, Ittner T, Nordqvist R, 1992, Aspo Hard Rock Laboratory. Evaluation of the combined longterm pumping and tracer test (LPT-2) in borehole KAS06. SKB, Technical Report 92-32.

Shimogaki H, Igarashi T, 1993, Leaching and migration model of trace elements from fly-ash disposal sites. Geoconfine '93, Montpellier, France, pp 123-128.

Svensson U, 1991a, Groundwater flow at Aspo and changes due to the excavation of the laboratory. SKB, Progress Report 25-91-03.

Svensson U, 1991b, Predictions of flow trajectories for the LPT-2 test. SKB, Progress Report 25-91-17

Wikberg P, Gustafson G, Rhen I, Stanfors R, 1991, Aspo Hard Rock Laboratory. Evaluation and conceptual modelling based on the pre-investigations 1986-1990. SKB, Technical Report 91-22.

Yeh G T, Ward D S, 1979, FEMWATER. A finite-element model of water flow through saturated-unsaturated porous media. ORNL-5567.

Yeh G H, Ward D S, 1981, FEMWASTE. A finite-element model of waste transport through saturated-unsaturated porous media. ORNL-5601.

APPENDIX

Model and code specification

- Name, version, and origin of the code

FEGM (Finite-Element model of groundwater Movement) / FERM (Finite-Element model of Radionuclide Migration) version 2

Origin of the codes is FEMWATER/FEMWASTE developed by Yeh *et al.*

- General description

Steady-state and unsteady-state groundwater flow including an unsaturated zone can be simulated by FEGM. The spatial dimensions can be arbitrarily selected, and the heterogeneity due to fractures can also be treated by a coupled smeared fracture model. Steady-state and unsteady-state solute transport with the groundwater flow calculated by FEGM can be simulated by FERM. The spatial dimensions and adsorption models can be arbitrarily selected, and the heterogeneity due to fractures can also be treated by a coupled smeared fracture model.

- Conceptual and mathematical model

The governing equation of FEGM is derived from continuity of fluid and solid, motion of fluid based on Darcy's law, consolidation of the medium, and compressibility of fluid. The governing equation of FERM is derived from mass balance considering convection, dispersion, diffusion, adsorption, radioactive decay, and decomposition.

- Numerical method

FEGM and FERM are based on the finite-element method. The matrix solver consists of the Banded matrix method, the Skyline matrix method, and the Conjugate gradient method.

-Limitation

The effects of salinity and temperature on the groundwater flow cannot be considered due to the assumption that the density of groundwater is constant. Random hydraulic conductivities having a log-normal distribution cannot be generated, and a different-aperture model is not included.

-Parameter required

Required parameters are similar to the parameters for a conventional deterministic groundwater flow model and a solute transfer model. When determining the groundwater

flow in an unsaturated zone, the relationship between suction potential and volumetric water content and the relationship between unsaturated hydraulic conductivity coefficient and volumetric water content should be taken into account.

-Type of results

Pressure head, total head, and Darcy velocity are obtained at a specific time with FEGM. Trajectories from arbitrary positions and fluxes that pass through arbitrary elements are also calculated with FEGM. On the other hand, concentration distribution at a specific time and concentration change at a specific point are obtained with FERM.

-Computer requirements

FEGM/FERM has been developed in Fortran 77, and is applicable to most workstations if the OS is Unix.

-User interface

FIDAP and ATLAS are used as a pre-processor and a post-processor.

-Code availability

FEGM/FERM has not yet been released. However, this code is available through CRIEPI, contingent on permission from the Japanese electric utilities.

List of International Cooperation Reports

ICR 93-01
Flowmeter measurement in borehole KAS 16
P Rouhiainen
June 1993
Supported by TVO, Finland

ICR 93-02
Development of ROCK-CAD model for Äspö Hard Rock Laboratory site
Pauli Saksa, Juha Lindh, Eero Heikkinen
Fintact KY, Helsinki, Finland
December 1993
Supported by TVO, Finland

ICR 93-03
Scoping calculations for the Matrix Diffusion Experiment
Lars Birgersson[1], Hans Widén[1], Thomas Ågren[1], Ivars Neretnieks[2], Luis Moreno[2]
1 Kemakta Konsult AB, Stockholm, Sweden
2 Royal Institute of Technology, Stockholm, Sweden
November 1993
Supported by SKB, Sweden

ICR 93-04
Scoping calculations for the Multiple Well Tracer Experiment - efficient design for identifying transport processes
Rune Nordqvist, Erik Gustafsson, Peter Andersson
Geosigma AB, Uppsala, Sweden
December 1993
Supported by SKB, Sweden

ICR 94-01
Scoping calculations for the Multiple Well Tracer Experiment using a variable aperture model
Luis Moreno, Ivars Neretnieks
Department of Chemical Engineering and Technology, Royal Institute of Technology, Stockholm, Sweden
January 1994
Supported by SKB, Sweden

ICR 94-02
Äspö Hard Rock Laboratory. Test plan for ZEDEX - Zone of Excavation Disturbance EXperiment. Release 1.0
February 1994
Supported by ANDRA, NIREX, SKB

ICR 94-03
The Multiple Well Tracer Experiment - Scoping calculations
Urban Svensson
Computer-Aided Fluid Engineering
March 1994
Supported by SKB, Sweden

ICR 94-04
Design constraints and process discrimination for the Detailed Scale Tracer Experiments at Äspö - Multiple Well Tracer Experiment and Matrix Diffusion Experiment
Jan-Olof Selroos[1], Anders Winberg[2], Vladimir Cvetkovic[2]
1 Water Resources Eng., KTH
2 Conterra AB
April 1994
Supported by SKB, Sweden

ICR 94-05
Analysis of LPT2 using the Channel Network model
Björn Gylling[1], Luis Moreno[1], Ivars Neretnieks[1], Lars Birgersson[2]
1 Department of Chemical Engineering and Technology, Royal Institute of Technology, Stockholm, Sweden
2 Kemakta Konsult AB, Stockholm, Sweden
April 1994
Supported by SKB, Sweden

ICR 94-06
SKB/DOE geochemical investigations using stable and radiogenic isotopic methods - First year
Bill Wallin[1], Zell Peterman[2]
1 Geokema AB, Lidingö, Sweden
2 U.S. Geological Survey, Denver, Colorado, USA
January 1994
Supported by SKB and U.S.DOE

ICR 94-07

Analyses of LPT2 in the Äspö HRL with continuous anisotropic heterogeneous model

Akira Kobayashi[1], Ryo Yamashita[2], Masakazu Chijimatsu[2], Hiroyuki Nishiyama[3], Yuzo Ohnishi[3]
1 Iwate University, Iwate, Japan
2 Hazama Corporation, Ibaraki, Japan
3 Kyoto University, Kyoto, Japan
September 1994
Supported by PNC, Japan

ISSN 1104-3210
ISRN SKB-ICR--94/8--SE
CM Gruppen AB, Bromma 1994